Microgravity Science and Technology
https://doi.org/10.1007/s12217-019-9690-5

ORIGINAL ARTICLE

# Numerical Simulation of Quasi-Static Bubble Formation from a Submerged Orifice by the Axisymmetric VOSET Method

Tai Wang[1] · Hui-Xiong Li[2] · Jian-Fu Zhao[3] · Kai-Kai Guo[2]

Received: 2 December 2018 / Accepted: 18 February 2019


## Abstract

In order to investigate the dynamics of quasi-static bubble formation from a submerged orifice, this paper developed an axisymmetric VOSET method with continuum surface force (CSF) model which can accurately capture the moving phase interface of gas-liquid flow. Test case shows that numerical results are in good agreement with experimental results from the literature. The effects of gas flow rate, orifice size, surface tension, contact angle, liquid density, and gravitational acceleration on bubble shape, departure time and departure volume are investigated and analyzed. It is found that increase in orifice size, surface tension, and contact angle results in the increase in the capillary force resisting bubble detachment, which leads to larger departure time and departure volume. But there is a critical contact angle, and contact angle has no significance effect on the process of bubble formation and detachment, when it is smaller than the critical value. Buoyancy force promoting bubble detachment increases with the increase of liquid density and gravitational acceleration, which results in smaller departure time and departure volume. Also, the forming process of the neck shape of bubble bottom at the bubble detachment stage is observed, and the results show that the position of the smallest part of the neck approximately equals to the orifice radius $R_c$.

**Keywords** Axisymmetric VOSET method · Bubble formation · Bubble detachment · Static contact angle · Numerical simulation

## Introduction

Bubble formation and detachment are common physical phenomena, which exist widely in many engineering applications such as energy and power engineering, chemical engineering, environmental engineering, and space engineering. The investigations of bubble formation and detachment would be conducive to the developments of boiling heat transfer (Kim et al. 2015; Munro and Ban 2015; Wu et al. 2016), bubble columns (Zhang et al. 2012), gas-liquid separator (Movafaghian et al. 2000), etc. Thus it always attracts amount attentions from researchers, in which the influence of physical properties of fluid, gas flow rate, orifice size, and other conditions are investigated by experimental observations, theoretical models, and numerical methods.

Because the process of bubble growth can be directly observed by visual experiments, amount of experimental work have been done. Bitlloch et al. (2018) presented the experimental results of air bubbles injected into water in microgravity. Zhang and Shoji (2001) experimentally investigated the influence of gas flow rate on aperiodic bubble formation from a submerged orifice, and found three types of bubble departing periods such as single period, double periods, and triple periods. Similar experimental researches were also performed in the literature (Badam et al. 2007; Buwa et al. 2007), and the effect of the orifice size, contact angle, and surface tension on the transitions of bubbling regimes with the increase of the gas flow rate was studied. For periodic bubble formation, gas flow rate has an important effect on the bubble dynamics. But when the gas flow rate is lower than the critical value $Q_{crit}$ from the literature (Oguz and Prosperetti 1993), the effect of the viscous stresses is very small, which is known as quasi-static bubble formation. Gerlach et al. (2005), Lesage and Marois (2013), Di Bari and Robinson (2013), Albadawi et al. (2013) presented some experimental investigations on the bubble shape, departure time and departure volume of

✉ Tai Wang
wangtai_1986@163.com

[1] School of Energy, Power and Mechanical Engineering, North China Electric Power University, Baoding 071003, China

[2] State Key Laboratory of Multiphase Flow in Power Engineering, Xi'an Jiaotong University, Xi'an 710049, China

[3] CAS Key Laboratory of Microgravity, Institute of Mechanics, Chinese Academy of Sciences, Beijing 100190, China

Published online: 06 March 2019

quasi-static bubble formation. Based on the experimental investigations, various theoretical models were also proposed. Zhang and Shoji (2001) developed a theoretical model which can predict the departing periods of bubble formation with single period to triple periods, which were in good agreement with the experimental results. Gerlach et al. (2005) presented two theoretical models which can predict the quasi-static bubble formation on the wettable and nonwettable surfaces. Vafaei et al. (2010), Das et al. (2011), and Lesage et al. (2013) also developed theoretical models based on different laws, and done the theoretical analysis of bubble formation.

In addition to the experimental observations and theoretical models, numerical simulation is another important method of studying bubble formation, and it can provide accurate predictions for bubble behaviors under various operating conditions. Simmons et al. (2015) utilized finite element method to simulate bubble formation from a submerged orifice, and the results showed that this method can capture the pinch-off of the bubble. Wu et al. (2017) investigated bubble formation under constant pressure conditions using a 3D boundary element method. Mirsandi et al. (2018) used the front tracking method with local front reconstruction technique and dynamic contact angle models to study bubble formation under various gas injection rates. Compared to the above mentioned methods, the Volume of Fluid (VOF) method (Hirt and Nichols 1981), Level Set (LS) method (Osher and Sethian 1988), and Combined LS and VOF method (CLSVOF) (Sussman and Puckett 2000) are more widely used in the investigations on bubble dynamics, especially the CLSVOF method combining the advantages of VOF and LS method. Ma et al. (2012), Hanafizadeh et al. (2015), and Georgoulas et al. (2015) applied VOF method to investigate bubble formation and detachment, and the effects of physical properties, operation conditions, gravity levels, and gravity vector direction were analyzed. Arias and Montlaur (2018) used VOF method to investigate the influence of the contact angle on the bubble generation from a capillary T-junction. Chen et al. (2009) studied the effect of the contact angle on bubble departure diameter using LS method with contact line models. Buwa et al. (2007) and Gerlach et al. (2007) used CLSVOF method to investigate the periodic bubble formation and analyze the transition of single period to double period. Similarly, periodic bubble formation in high-density liquid was also investigated by Chakraborty et al. (2015) using the CLSVOF method. And, the same numerical method was also used to study the quasi-static bubble formation by Albadawi et al. (2013). Chakraborty et al. (2009) applied CLSVOF method to simulate the process of bubble formation under normal and reduced gravity, and found that the detached bubble volume significantly increases with the decrease of gravity.

As another coupling method, VOSET method (Sun and Tao 2010) can also combine the advantages of VOF and LS method. Over the past few years, VOSET method has been developed to investigate complicated multiphase flow problems, such as boiling (Guo et al. 2011), ferrofluid droplet dynamics (Shi et al. 2014), bubble dynamics (Wang et al. 2016), etc. In this paper, the VOSET method was performed on the axisymmetric coordinate system, which is used to simulate quasi-static bubble formation from a submerged orifice in quiescent viscous fluids. Different mesh sizes are utilized to carry out grid independence verification, and the numerical results are validated by the experimental results from literature (Albadawi et al. 2013). The influence of gas flow rate, orifice size, surface tension, contact angle, liquid density, and gravitational acceleration on bubble shape, departure time and departure volume are investigated.

## Numerical Formulation

### Governing Equations

In the present study, the process of bubble formation from a single submerged orifice in a quiescent liquid is expected to be axisymmetric, hence the cylindrical axisymmetric coordinate system $(r, z)$ is created. The dispersed phase (gas) and continuous phase (liquid) are assumed to be immiscible, incompressible, and Newtonian fluid. The continuity equation, Navier-Stokes equations, and interface capturing advection equation are solved for the two-phase flow as:

$$\nabla\cdot\boldsymbol{U} = 0 \tag{1}$$

$$\frac{\partial(\rho\boldsymbol{U})}{\partial t} + \nabla\cdot(\rho\boldsymbol{U}\boldsymbol{U}) = -\nabla p + \rho\boldsymbol{g} + \nabla\cdot\left[\mu\left((\nabla\boldsymbol{U}) + (\nabla\boldsymbol{U})^T\right)\right] + \boldsymbol{F}_\sigma \tag{2}$$

$$\frac{\partial C}{\partial t} + \boldsymbol{U}\cdot\nabla C = 0 \tag{3}$$

where $\boldsymbol{U}$ is the velocity vector, $p$ is the pressure, $\rho$ is the fluid density, $\mu$ is the fluid viscosity, $\boldsymbol{g}$ is the gravitational acceleration, $\boldsymbol{F}_\sigma$ is the surface tension force, and $C$ is the volume fraction as the fraction of the gas in a cell.

For the $(r, z)$ coordinate system, the continuity equation and Navier-Stokes equations can be rewritten as:

$$\frac{1}{r}\frac{\partial(ru)}{\partial r} + \frac{\partial v}{\partial z} = 0 \tag{4}$$

$$\frac{\partial(\rho u)}{\partial t}+\frac{\partial}{\partial z}\left(\rho vu-\mu\frac{\partial u}{\partial z}\right)+\frac{1}{r}\frac{\partial(r\rho uu)}{\partial r}$$
$$=-\frac{\partial p}{\partial r}+\rho g_r+\frac{\partial}{\partial z}\left(\mu\frac{\partial v}{\partial r}\right)+\frac{2}{r}\frac{\partial}{\partial r}\left(r\mu\frac{\partial u}{\partial r}\right)-\frac{2\mu u}{r^2}+F_{\sigma r} \tag{5}$$

$$\frac{\partial(\rho v)}{\partial t}+\frac{\partial(\rho vv)}{\partial z}+\frac{1}{r}\frac{\partial}{\partial r}\left(r\rho uv-r\mu\frac{\partial v}{\partial r}\right)$$
$$=-\frac{\partial p}{\partial z}+\rho g_z+2\frac{\partial}{\partial z}\left(\mu\frac{\partial v}{\partial z}\right)+\frac{1}{r}\frac{\partial}{\partial r}\left(r\mu\frac{\partial u}{\partial z}\right)+F_{\sigma z} \tag{6}$$

where $u$ is the radial velocity, $v$ is the axial velocity. The surface tension force is calculated by the continuum surface force (CSF) model (Brackbill et al. 1992).

$$F_{\sigma r}=-\sigma\kappa\delta(\phi)\frac{\partial\phi}{\partial r},\quad F_{\sigma z}=-\sigma\kappa\delta(\phi)\frac{\partial\phi}{\partial z} \tag{7}$$

where $\sigma$ is the surface tension coefficient, $\phi$ is the level set function, and $\kappa$ is the interface curvature which can be computed as:

$$\kappa=\nabla\cdot\left(\frac{\nabla\phi}{|\nabla\phi|}\right) \tag{8}$$

For the $(r, z)$ coordinate system, the interface curvature can be rewritten as:

$$\kappa=\left[\frac{\partial^2\phi}{\partial z^2}\left(\frac{\partial\phi}{\partial r}\right)^2-2\frac{\partial^2\phi}{\partial z\partial r}\frac{\partial\phi}{\partial z}\frac{\partial\phi}{\partial r}+\frac{\partial^2\phi}{\partial r^2}\left(\frac{\partial\phi}{\partial z}\right)^2\right]/\left[\sqrt{\left(\frac{\partial\phi}{\partial r}\right)^2+\left(\frac{\partial\phi}{\partial z}\right)^2}\right]^3$$
$$+\left[\frac{1}{r}\frac{\partial\phi}{\partial r}/\sqrt{\left(\frac{\partial\phi}{\partial r}\right)^2+\left(\frac{\partial\phi}{\partial z}\right)^2}\right] \tag{9}$$

And, $\delta(\phi)$ is the Dirac distribution function which is expressed as:

$$\delta(\phi)=\begin{cases}0 & \text{for } |\phi|>\varepsilon\\ \frac{1}{2\varepsilon}\left[1+\cos\left(\frac{\pi\phi}{\varepsilon}\right)\right] & \text{for } |\phi|\le\varepsilon\end{cases} \tag{10}$$

where $\varepsilon = 1.5\Delta$ is the width of the smoothed region, $\Delta$ is the grid size.

The gas density $\rho_g$, gas viscosity $\mu_g$, liquid density $\rho_l$, and liquid viscosity $\mu_l$ are assumed to be constant, and the density $\rho$ and viscosity $\mu$ of two-phase fluid are calculated by

$$\rho=\rho_l H(\phi)+\rho_g(1-H(\phi)) \tag{11}$$

$$\mu=\mu_l H(\phi)+\mu_g(1-H(\phi)) \tag{12}$$

where $H(\phi)$ is the Heaviside function which is expressed as:

$$H(\phi)=\begin{cases}0 & \text{for } \phi<-\varepsilon\\ \frac{1}{2}\left[1+\frac{\phi}{\varepsilon}+\frac{1}{\pi}\sin\left(\frac{\pi\phi}{\varepsilon}\right)\right] & \text{for } |\phi|\le\varepsilon\\ 1 & \text{for } \phi>\varepsilon\end{cases} \tag{13}$$

## The VOSET Method

The coupled volume-of-fluid and level set (VOSET) method (Sun and Tao 2010) is implemented on the axisymmetric coordinate system in the present study. In the VOSET method, the advection equation (Eqs. (3)) of the volume fraction $C$ is solved by the PLIC algorithm (Youngs 1982) and unsplit advection scheme (Wang et al. 2013), which is used to capture the two-phase interface. But, the advection equation of the level set function $\phi$ does not need to be solved. A geometric method is used to calculate $\phi$ which is used to accurately calculate interface normal and curvature. The detailed operation procedure of the VOSET method is presented as follows:

Step 1: Reconstruct the interface by the PLIC algorithm according to the volume fraction $C$ and normal vector $\boldsymbol{n}$. The normal vector $\boldsymbol{n}$ is calculated by

$$\boldsymbol{n}=\frac{\nabla C}{|\nabla C|} \tag{14}$$

In the PLIC algorithm, there are many possible interface cases. In order to simplify the calculation of the interface equation, coordinate transformation is used to reduce the number of the interface cases. The simplified interface cases include four types as shown in Fig. 1a. To calculate the interface equation, a new coordinate system $(r', z')$ on the multi-material cell $(0 < C < 1)$ is established. So, the interface equation in Fig. 1b can be expressed as:

$$n_{r'}\left(r'-r'_A\right)+n_{z'}z'=0 \tag{15}$$

where $n_{r'} > 0$ and $n_{z'} > 0$ are the radial and axial components of the normal vector $\boldsymbol{n}$, respectively. $(r'_A, 0)$ is the coordinate of point A.

According to the definition of the volume fraction $C$, it can be calculated by

$$C=\frac{1}{V_{ODGF}}(V_{OAB}-\zeta_1 V_{ACD}-\zeta_2 V_{BEF}) \tag{16}$$

where $V_{ODGF}$ is the volume of a ring with rectangular cross section in cylindrical coordinates, and $V_{OAB}$, $V_{ACD}$, $V_{BEF}$ are

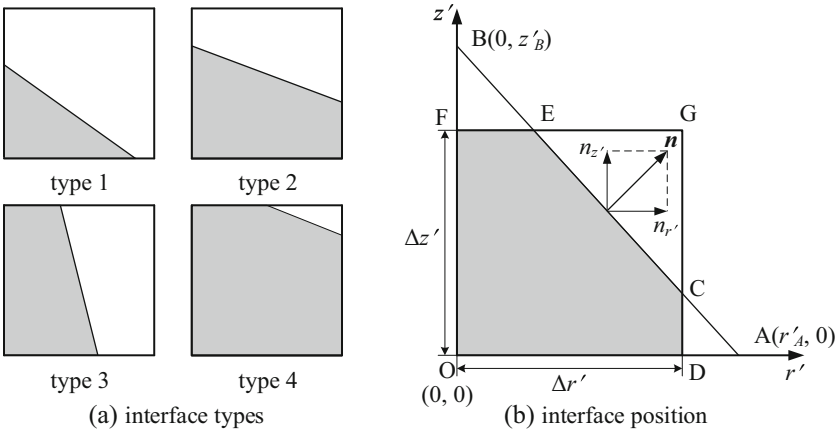


**Fig. 1** Schematic of interface types and position

the volume of a ring with triangular cross section. The equation coefficient $\zeta_1$ and $\zeta_2$ are computed as:

$$\zeta_1 = \begin{cases} 0, & \text{for type 1 and type 3 of the interface} \\ 1, & \text{for type 2 and type 4 of the interface} \end{cases} \tag{17}$$

$$\zeta_2 = \begin{cases} 0, & \text{for type 1 and type 2 of the interface} \\ 1, & \text{for type 3 and type 4 of the interface} \end{cases} \tag{18}$$

The coordinate of point A can be calculated by Eqs. (16–18), which is used to determine the interface equation.

Step 2: Set up the initial level set function $\phi$ in the whole computational domain.

$$\phi_{i,j}^0 = \begin{cases} -L, & \text{for cell center in the gas phase} \\ 0, & \text{for cell center on the interface} \\ L, & \text{for cell center in the liquid phase} \end{cases} \tag{19}$$

where $L = \max(L_r, L_z)$ is the max size of the computational domain $(L_r, L_z)$.

Step 3: Mark the cells in $4\Delta$ region near the interface as shown in Fig. 2a. Because the level set function $\phi$ is only used to calculate the surface tension force and fluid physical quantities. Thus, only the level set function $\phi$ on the marked cells need to be calculated, which can save computing resources.

Step 4: Calculate the level set function $\phi$ on each marked cell. Firstly, we should determine a $7 \times 7$ stencil around the marked cell, as shown in Fig. 2b. Subsequently all of the minimum distances from cell center point $P$ to any interface in cells within the stencil are calculated. As shown in Fig. 3, if point $M$ is between point $A$ and point $B$, $d_{PM}$ is the minimum distance, otherwise $\min(d_{PA}, d_{PB})$ is the minimum distance. For all of the minimum distances, the minimum value is the shortest distance $d$ from point $P$ to the interface. Then, the level set function $\phi$ can be expressed as:

$$\phi = \begin{cases} -d, & \text{for } \phi_{i,j}^0 < 0 \\ 0, & \text{for } \phi_{i,j}^0 = 0 \\ d, & \text{for } \phi_{i,j}^0 > 0 \end{cases} \tag{20}$$

Based on the level set function $\phi$, the normal vector $\boldsymbol{n}$ is calculated by

$$\boldsymbol{n} = \frac{\nabla\phi}{|\nabla\phi|} \tag{21}$$

Then, return to *Step* 1. The interface is reconstructed by the Eqs. (21) with higher accuracy. The iteration times in the present study is set as 3. Figure 4 shows the level set function $\phi$ near the interface of a circular bubble, which denotes that the level set function $\phi$ can be accurately calculated by the iterative geometric operation. For the circular bubble, the interface curvature are calculated by the VOSET method and VOF method. Table 1 shows the $L_2$ error norm for curvature, in which $N$ is the number of the multi-material cells. It can be seen that the VOSET method has higher calculation accuracy.

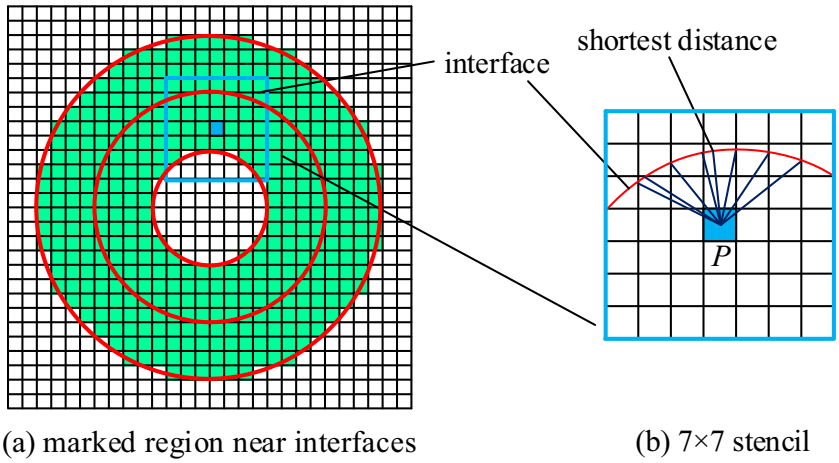


**Fig. 2** Schematic of the marked region near interfaces and the shortest distance

## Computational Domain and Boundary Conditions

Due to the axisymmetric physical model, the computational domain is chosen as 1 rad (as shown in Fig. 5). The computational domain should be sufficient to ensure that the bubble dynamics are independent of domain size. In the present study, the width and height are considered to be $L_r \geq 2.5D_{det}$ and $L_z \geq 5D_{det}$, where $D_{det}$ is the bubble equivalent diameter. The gas is injected through an orifice of radius $R_c$ with a constant flow rate $Q$. The axisymmetric boundary condition, the slip boundary condition, and Neumann boundary condition are applied at the symmetry axis ($r = 0$), side boundary ($r = L_r$) and outlet ($z = L_z$), respectively. Additionally, the bottom solid wall is set to be no slip boundary condition, and the wall static contact angle is $\theta$. In the static contact angle model, the angle $\theta$ is used to calculate the level set function $\phi$ on the bottom boundary by using the Eqs. (22). Then, the curvature and surface tension force near the contact line are calculated by the Eqs. (7–9).

$$\cos\theta = -\frac{\partial\phi}{\partial z} \tag{22}$$

## Numerical Validation

### Grid Independence Verification

In order to test the effect of grid size on numerical results, simulation of quasi-static bubble formation from a submerged orifice in a pure water is performed using different uniform grid systems ($R_c/\Delta = 4$, 8, 16, and 24). The density and viscosity of the gas are $\rho_g = 1.225$ kg·m$^{-3}$ and $\mu_g = 1.79 \times 10^{-5}$ kg·(m·s)$^{-1}$. And, the density and viscosity of the water are $\rho_w = 998.2$ kg·m$^{-3}$ and $\mu_w = 1.0 \times 10^{-3}$ kg·(m·s)$^{-1}$. The surface tension coefficient $\sigma_{gw}$ equals to 0.073 N·m$^{-1}$, and the contact angle $\theta$ is set to be 30°. The comparisons for

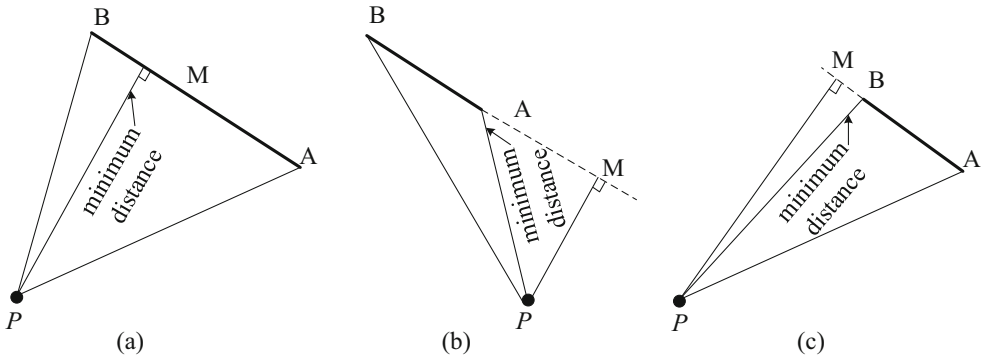


**Fig. 3** The minimum distance to an interface in a cell

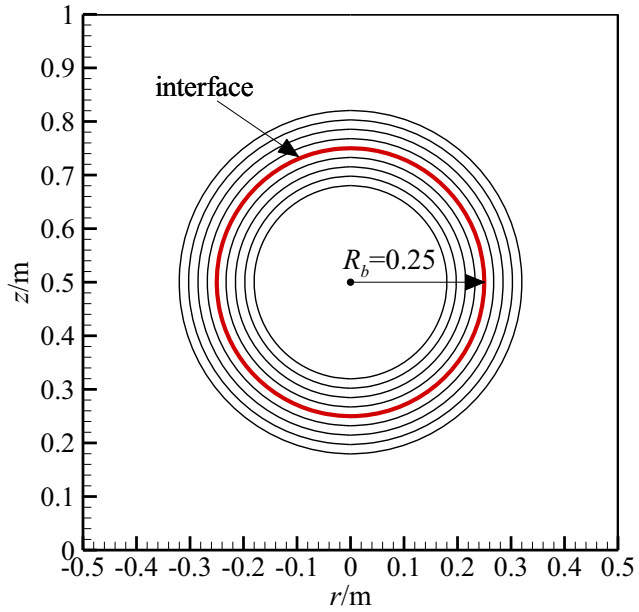


**Fig. 4** The level set function near the interface of a circular bubble

bubble departure volume $V_{det}$ and departure diameter $D_{det}$ under the condition of $R_c = 0.8$ mm and $Q = 200$ ml/h are shown in Table 2, in which the error $E_V$ and $E_D$ are calculated by the following formula.

$$E_V = \frac{V_{det,R_c/\Delta=24} - V_{det,R_c/\Delta=4,8,16,24}}{V_{det,R_c/\Delta=24}} \times 100\% \tag{23}$$

$$E_D = \frac{D_{det,R_c/\Delta=24} - D_{det,R_c/\Delta=4,8,16,24}}{D_{det,R_c/\Delta=24}} \times 100\% \tag{24}$$

Table 2 shows the results of four cases, it can be seen that bubble departure volume $V_{det}$ and departure diameter $D_{det}$ gradually increase, but the difference of two adjacent cases gradually decreases with the increase of $R_c/\Delta$. Obviously, case A has the largest error $E_V = 14.61\%$ and $E_D = 5.19\%$. Although case B can improve the calculation accuracy, $E_V =$ 5.31% is still a large error. Compared to case A and case B, case C has smaller errors, and the difference between case C and case D is no significant. Thus, the grid size $R_c/\Delta$=16 m is adopted in the present study due to considering the accuracy of calculation and the cost of computer resources.

### Comparison of Numerical and Experimental Results

To verify the accuracy of the numerical results, comparison of bubble shape in different time $t/t_{det}$ for the case C in Table 2 and the experimental results reported by Albadawi et al. (2013) are performed in this section. As shown in Fig. 6, bubble shape predicted by the axisymmetric VOSET method can be in good agreement with experimental observations. For the bubble departure volume, the numerical and experimental results are 29.36 mm$^3$ and 30.074 mm$^3$ respectively, and the relative error is 2.37%. Therefore, it can be concluded that the axisymmetric VOSET method can be adopted to simulated quasi-static bubble formation.

## Results and Discussions

This section presents the numerical results of the effects of gas flow rate, orifice size, surface tension, contact angle, liquid density, and gravitational acceleration on quasi-static bubble formation from a submerged orifice. To describe bubble behaviors, the following parameters are defined.

$$\lambda_g = \frac{g}{g_0}, \quad \lambda_\rho = \frac{\rho_l}{\rho_w}, \quad \lambda_\mu = \frac{\mu_l}{\mu_w}, \quad \lambda_\sigma = \frac{\sigma_{gl}}{\sigma_{gw}} \tag{25}$$

where $g_0$ is terrestrial gravity which equals to 9.81 m/s$^2$. $\lambda_\rho$, $\lambda_\mu$, $\lambda_\sigma$ are the ratios of density, viscosity, and surface tension coefficient between the liquid adopted in this section and water. Physical properties of gas and water can be found in section 3.1, which keep constant in the following simulation. For all numerical examples in the present study, the gas flow rate

**Table 1** $L_2$ error norm for curvature estimated along a circular interface using the VOF and VOSET methods at different grid systems

| Case | $\Delta$ | $R_b/\Delta$ | $L_2 = \sqrt{\sum_i^N (\kappa_i \times R/2 - \kappa_{exacct} \times R/2)^2 / N}$ | |
|---|---|---|---|---|
| | | | VOF | VOSET |
| A | 1/20 | 5 | 0.164 | $2.11 \times 10^{-2}$ |
| B | 1/40 | 10 | 0.236 | $1.72 \times 10^{-2}$ |
| C | 1/80 | 20 | 0.428 | $1.17 \times 10^{-2}$ |
| D | 1/160 | 40 | 0.885 | $1.35 \times 10^{-2}$ |
| E | 1/320 | 80 | 1.736 | $1.81 \times 10^{-2}$ |

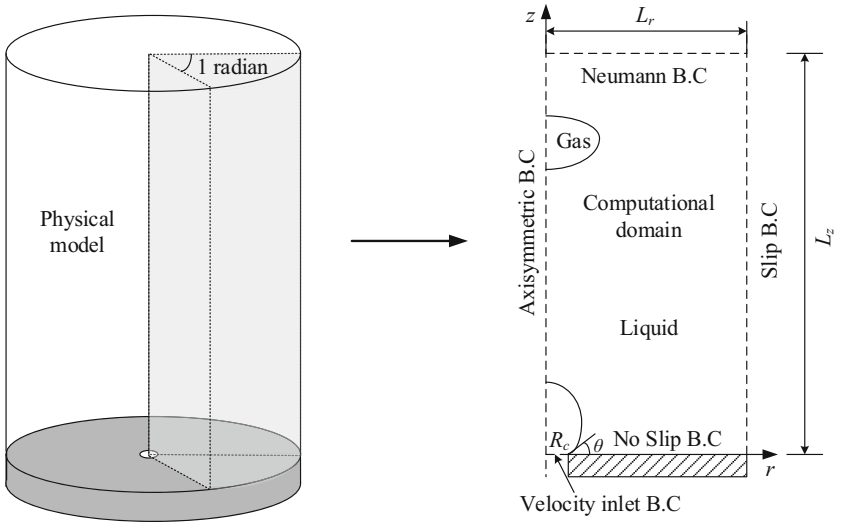


**Fig. 5** Schematic illustrations of physical model and computational domain

is lower than the critical value $Q_{crit}$ which is calculated by the following equation (Oguz and Prosperetti 1993).

$$Q_{crit} = \pi\left(\frac{16}{3g^2}\right)^{1/6}\left(\frac{\sigma_{gl}R}{\rho_l}\right)^{5/6} \tag{26}$$

## Influence of Gas Flow Rate

The effect of gas flow rate on the process of quasi-static bubble formation is shown in Fig. 7, where bubble shapes at different time $t/t_{det}$ are provided for $Q = 200$ ml/h and $Q = 1000$ ml/h with the conditions of $R_c = 1$ mm, $\lambda_g = 1$, $\lambda_\rho = 1$, $\lambda_\mu = 1$, $\lambda_\sigma = 1$, and $\theta = 30°$. As shown in Fig. 7a, a hemispherical bubble at the initial time located on the orifice, and gradually becomes a truncated tear shape ($t/t_{det} = 0.8$) with the increase of the bubble volume. During the detachment stage, the bubble bottom gradually shrinks and eventually becomes a neck shape. Compared with Fig. 7a, b presents a similar process of bubble formation and detachment, but the bubble size for $Q = 1000$ ml/h is a little bigger than $Q = 200$ ml/h which can also be observed in Fig. 8a and b. Besides the initial time, the bubble height $L$ for $Q = 1000$ ml/h is always higher than $Q = 200$ ml/h, and the differences gradually increases with $t/t_{det}$ changing from 0.0 to 0.9, but the detachment stage ($t/t_{det} > 0.9$) has an opposite trend owing to quickly bubble rising for $Q = 200$ ml/h. Also, the bubble width $M$ has the similar trend. It can also be seen that the position of the smallest part of the neck approximately equals to the orifice radius $R_c$, which is not significantly affected by the gas flow rate.

The effect of gas flow rate on bubble departure volume $V_{det}$, departure diameter $D_{det}$ and departure time $t_{det}$ is shown in Fig. 9. It can be seen that the bubble departure volume and departure diameter almost linearly increase with the gas flow rate during 200 ml/h and 1000 ml/h, and the increase rates are

**Table 2** Results of the grid-independent tests under the condition of $R_c = 0.8$ mm and $Q = 200$ ml/h

| Case | $R_c/\Delta$ | $\Delta$ (m) | $V_{det}$ (mm$^3$) | $D_{det}$ (mm) | $E_V$ (%) | $E_D$ (%) |
|---|---|---|---|---|---|---|
| A | 4 | $2.0 \times 10^{-4}$ | 25.42 | 3.65 | 14.61 | 5.19 |
| B | 8 | $1.0 \times 10^{-4}$ | 28.19 | 3.78 | 5.31 | 1.82 |
| C | 16 | $5.0 \times 10^{-5}$ | 29.36 | 3.83 | 1.38 | 0.52 |
| D | 24 | $3.3 \times 10^{-5}$ | 29.77 | 3.85 | 0 | 0 |

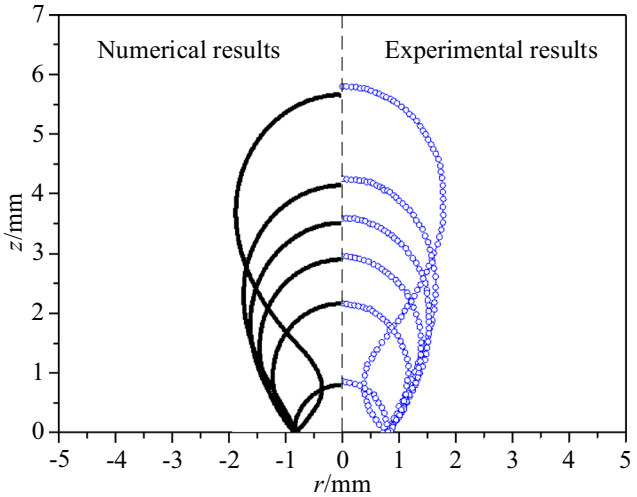


**Fig. 6** Bubble shape at different time $t/t_{det} = 0$, 0.2, 0.4, 0.6, 0.8, 1.0 of numerical results and experimental results (Albadawi et al. 2013)

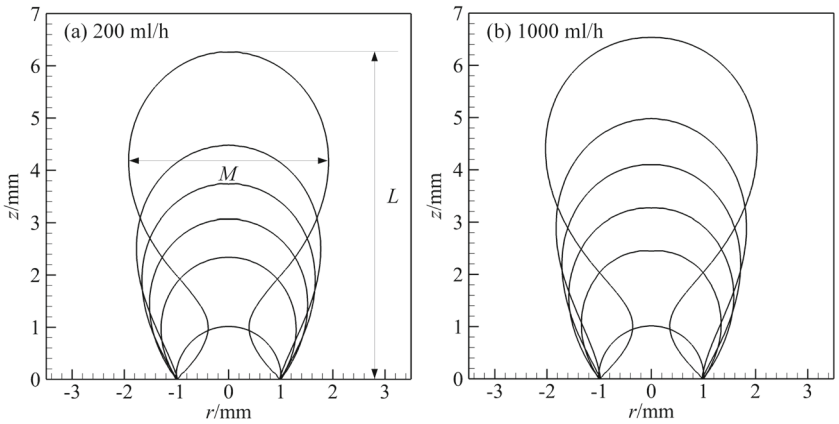


**Fig. 7** Bubble shapes at different time $t/t_{det} = 0$, 0.2, 0.4, 0.6, 0.8, 1.0 for $Q = 200$ ml/h and 1000 ml/h

0.716 mm$^3$/(100 ml/h) and 0.025 mm/(100 ml/h), respectively. Considering the previous investigations and the present results, it can be concluded that the effect of gas flow rate on the bubble shape, departure volume and departure diameter for quasi-static bubble formation is very small. Compared to other departure parameters, bubble departure time quickly decreases due to the fact that the variation of $V_{det}$ is much less than that of the gas flow rate.

Based on the experimental investigations of literature (Di Bari and Robinson 2013), it is known that for quasi-static bubble formation, four forces act on the bubble, in which capillary force and dynamic force resist bubble detachment, and contact pressure force and buoyancy force promote bubble detachment. Increase of gas flow rate results in the increase of dynamic force which needs to be overcome by a bigger buoyancy force, thus bubble departure volume increases. But because the dynamic force is much less than the capillary force, the effect of gas flow rate on bubble dynamics is no significant.

## Influence of Orifice Size

For quasi-static bubble formation, the primary force resisting bubble detachment is the capillary force affected by the orifice size, surface tension coefficient, and contact angle. The influence of orifice size is investigated in this section. Figure 10 shows the bubble shapes at different time for $R_c = 0.5$ mm and $R_c = 2.0$ mm with the conditions of $Q = 200$ ml/h, $\lambda_\rho = 1$, $\lambda_\mu = 1$, $\lambda_\sigma = 1$, $\lambda_g = 1.0$, and $\theta = 30°$. It can be seen that orifice size has significant influence on bubble shape. When orifice radius ($R_c = 0.5$ mm) is small, the ratio of bubble width $M$ and orifice radius $R_c$ gradually increases with time and reaches the largest value at $t/t_{det} = 1$. At the stage of bubble formation, the bubble is approximately tear shape. But for the larger orifice radius, the increase of the ratio $M/R_c$ is small, and the bubble is approximately semi-ellipsoidal shape. At the detachment stage, it can be found that the smallest part of the neck locates at the top of the initial bubble ($t/t_{det} = 0$), and the radius of the initial bubble equals to $R_c$. Thus, the larger orifice diameter leads to longer neck.

Figure 10 shows that the bubble size for $R_c = 2$ mm is more larger than that for $R_c = 0.5$ mm. And, the influence of orifice size on bubble departure volume $V_{det}$, departure diameter $D_{det}$ and departure time $t_{det}$ is shown in Fig. 11. It can be found that orifice size has significant effect on bubble departure parameters. Bubble departure volume linearly increases with the increase of orifice radius, and the increase rate is 35.63 mm$^3$/mm. The results also denotes that the capillary force and orifice radius is a positive linear relationship. Larger orifice radius leads to a larger capillary force which

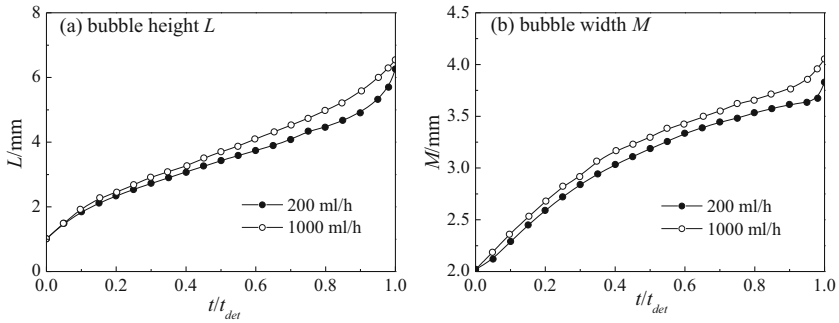


**Fig. 8** Bubble height and width versus time $t/t_{det}$ with $Q = 200$ ml/h and 1000 ml/h

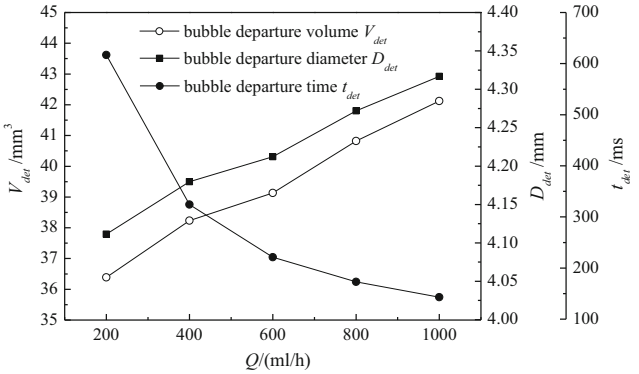


**Fig. 9** Effect of gas flow rate on bubble departure parameters

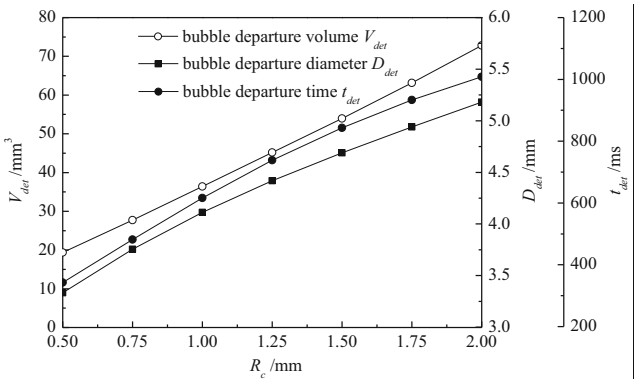


**Fig. 11** Effect of orifice size on bubble departure parameters

needs to be overcome by a larger buoyancy force. Thus, bubble departure diameter and departure time also increase with orifice radius.

## Influence of Surface Tension Coefficient

Surface tension coefficient is the main parameter controlling surface force keeping bubble shape and capillary force resisting bubble detachment. Thus, the influence of surface tension coefficient on bubble formation and detachment is investigated in this section. Bubble shapes at different time $t/t_{det}$ for $\lambda_\sigma = 0.25$ and $\lambda_\sigma = 1.5$ with the conditions of $Q = 200$ ml/h, $R_c = 1$ mm, $\lambda_\rho = 1$, $\lambda_\mu = 1$, $\lambda_g = 1.0$, and $\theta = 30°$ are shown in Fig. 12. It can be seen that for smaller surface tension coefficient ($\lambda_\sigma = 0.25$), smaller surface force leads to the decrease of the capacity of keeping bubble shape, thus the bubble width at the stage of bubble formation is similar to the orifice diameter under the pull effect of buoyancy force. Increase in surface tension coefficient results in the increase of the effect of the surface force, which leads to the gradually increase of the bubble width. It can also be found that bubble size for $\lambda_\sigma = 1.5$ is significantly larger than that for $\lambda_\sigma = 0.25$. As shown in Fig. 13, the effect of surface tension coefficient on bubble departure parameters is presented. Bubble departure volume, departure diameter and departure time increase with the increase of surface tension coefficient due to the increase of capillary force. Bubble departure volume has a liner relationship with surface tension coefficient, which denotes that increase in surface tension coefficient results in the liner increase of capillary force. Although surface tension coefficient is an important parameter, it has no significant effect on the position of the smallest part of the bubble neck.

## Influence of Contact Angle

The third parameter affecting capillary force is contact angle which is studied in this section. Figure 14 shows the effect of contact angle on bubble shape under the conditions of

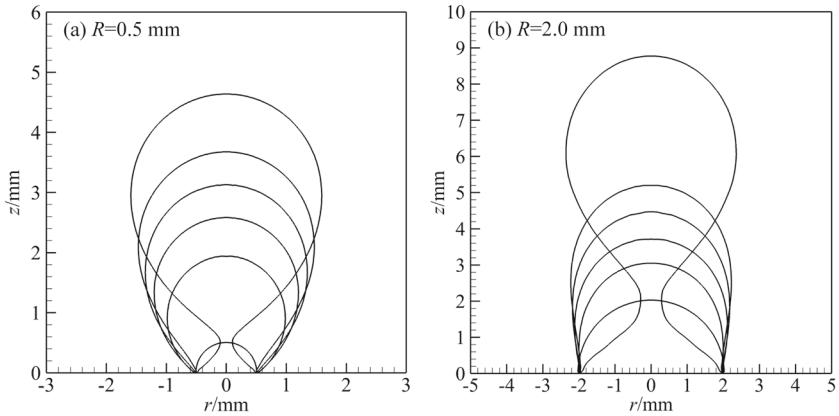


**Fig. 10** Bubble shapes at different time $t/t_{det} = 0$, 0.2, 0.4, 0.6, 0.8, 1.0 for $R_c = 0.5$ mm and 2.0 mm

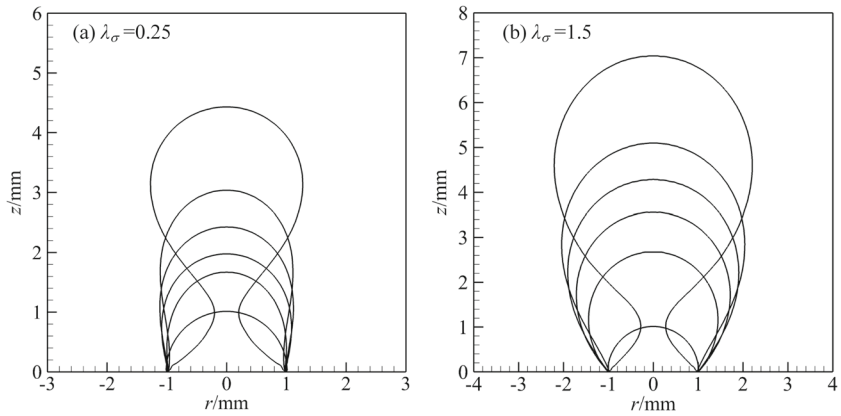


**Fig. 12** Bubble shapes at different time $t/t_{det} = 0$, 0.2, 0.4, 0.6, 0.8, 1.0 for $\lambda_\sigma = 0.25$ and 1.5

$Q = 200$ ml/h, $\lambda_\rho = 1$, $\lambda_\mu = 1$, $\lambda_\sigma = 1$, $\lambda_g = 1.0$, and $R_c = 1$ mm. It can be seen that at the same time $t/t_{det}$, bubble shapes for $\theta = 30°$ and $\theta = 45°$ have no significance difference, but slightly difference happens when contact angle is 60°. Carefully observed the bubble bottom, it can be found that the contact line for $\theta = 30°$ and $\theta = 45°$ is always fixed on the orifice edge, and the detailed changing of the positions of contact line with time $t/t_{det}$ for different contact angle are shown in Fig. 15. For $\theta = 60°$, contact line gradually moves outward with time $t/t_{det}$ from 0 to 0.45, and subsequently retracts with time $t/t_{det}$ from 0.45 to 0.85. As contact angle further increases, the distance of contact line away from the symmetry axis quickly increases, and the retracting of contact line is delayed. For $\theta = 75°$ and $\theta = 90°$, contact line retracts at the bubble detachment stage, in which $\theta = 90°$ has a more steep curve. It can also be found that contact angle has no significant effect on the position of the smallest part of the bubble neck.

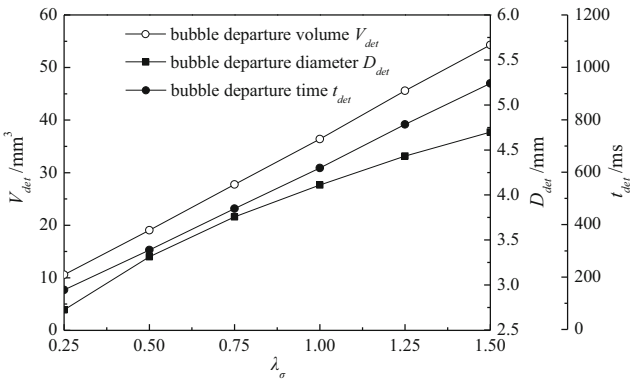


**Fig. 13** Effect of surface tension coefficient on bubble departure parameters

The effect of contact angle on bubble departure volume $V_{det}$, departure diameter $D_{det}$ and departure time $t_{det}$ is shown in Fig. 16. It can be seen that when contact angle is lower than 60°, contact angle has no significance influence on bubble departure parameters. But, for contact angle increasing from 60° to 90°, bubble departure volume, departure diameter and departure time quickly increase. The results denote that there is a critical value of the contact angle to distinguish the effect of capillary force by changing contact angle.

## Influence of Liquid Density

The primary force promoting bubble detachment is the buoyancy force affected by the liquid density, gravitational acceleration and bubble volume, and the effect of liquid density is investigated in this section. Bubble shapes at different time $t/t_{det}$ for $\lambda_\rho = 0.8$ and $\lambda_\rho = 2.0$ under the conditions of $Q = 200$ ml/h, $R_c = 1$ mm, $\lambda_\mu = 1$, $\lambda_\sigma = 1$, $\lambda_g = 1.0$, and $\theta = 30°$ are shown in Fig. 17. It can be seen that the bubble size for $\lambda_\rho = 0.8$ is far larger than that for $\lambda_\rho = 2.0$. The bubble width for $\lambda_\rho = 0.8$ quickly increases with time, which is more larger than the case for $\lambda_\rho = 2.0$ owing to the increase of the pull effect of buoyancy force. Though different liquid density results in different bubble shapes, liquid density has no significance effect on the position of the smallest bubble neck.

With the increase of liquid density, achieving the same buoyancy force needs a smaller bubble volume, which results in the decrease of the bubble departure volume, departure diameter and departure time. And, the changing curves of liquid density on bubble departure volume $V_{det}$, departure diameter $D_{det}$ and departure time $t_{det}$ are shown Fig. 18. It can be seen that the curves are not linear and

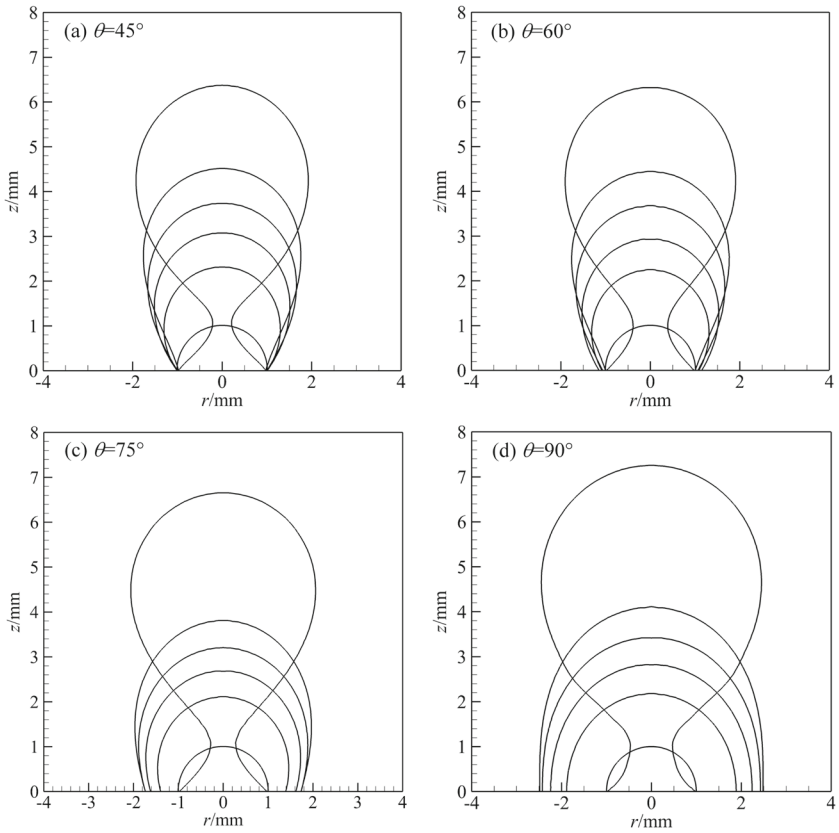


**Fig. 14** Bubble shapes at different time $t/t_{det} = 0$, 0.2, 0.4, 0.6, 0.8, 1.0 for different contact angle

the curvature gradually decreases, which denotes that when liquid density is small, the changing of liquid density has more effect on bubble departure parameters.

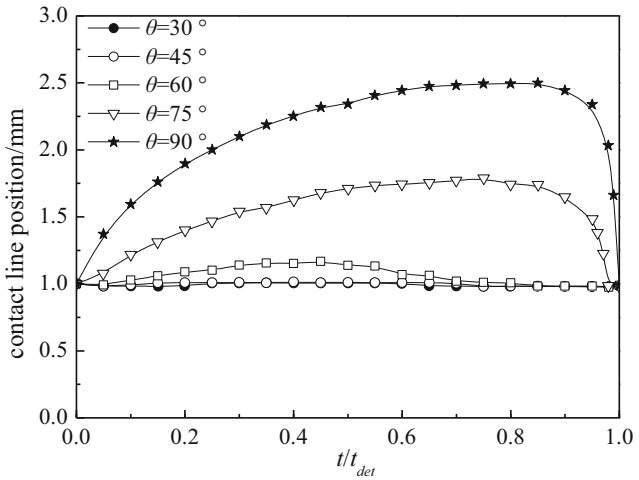


**Fig. 15** Distance between contact line and symmetry axis changing with time $t/t_{det}$ for different contact angle

## Influence of Gravitational Acceleration

In the space engineering, spacecraft operates in different gravity environments, and the gravity level has significant influence on bubble dynamics, two-phase flow, and heat transfer (Pang et al. 2017; Zhang et al. 2018). Thus, the effect of gravitational acceleration on quasi-static bubble formation is investigated in this section. Figure 19 shows

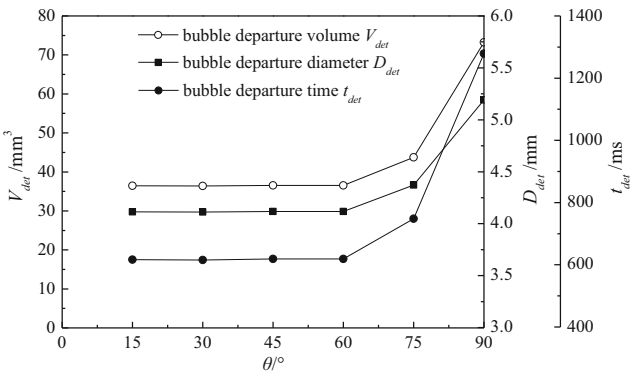


**Fig. 16** Effect of contact angle on bubble departure parameters

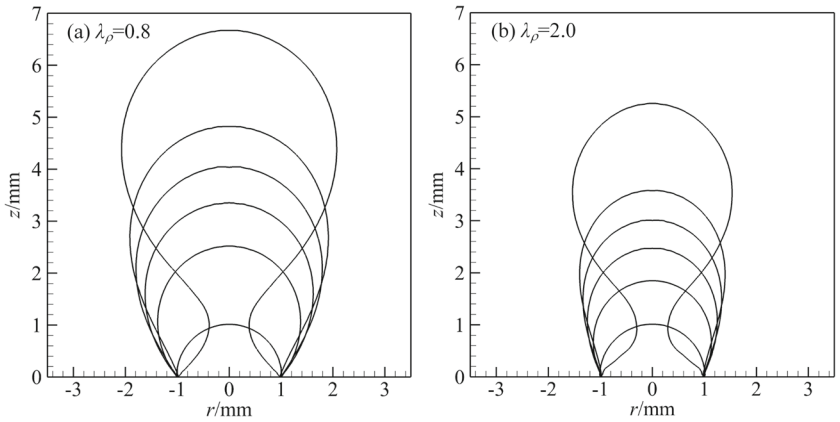


**Fig. 17** Bubble shapes at different time $t/t_{det} = 0$, 0.2, 0.4, 0.6, 0.8, 1.0 for $\lambda_\rho = 0.8$ and 2.0

bubble shapes at different time $t/t_{det}$ for different gravitational acceleration under the conditions of $Q = 200$ ml/h, $\lambda_\rho = 1$, $\lambda_\mu = 1$, $\lambda_\sigma = 1$, and $\theta = 30°$. It can be seen that when $\lambda_g$ equals to 0.25, the bubble width at the stage of bubble formation and detachment gradually increases, and the bubble width for $t/t_{det} = 1$ is far lager than the orifice diameter. When $\lambda_g$ increases to 0.75, the bubble width and height at the same time $t/t_{det}$ obviously decrease owing to the increase of the effect of buoyancy force. With the further increase of gravitational acceleration, the bubble width and height further decrease. Especially for $\lambda_g = 4$, the bubble width at different time is very close to the orifice diameter. Observed the neck of bubble bottom, it can also be found that gravitational acceleration has no significance effect on the position of the smallest part of the neck.

Figure 20 shows the effect of gravitational acceleration on bubble departure volume, departure diameter and departure time. Compared to Fig. 18, it can be found that gravitational acceleration has the same influence on bubble departure parameters with the liquid density. The fact is that departure parameters gradually decrease with the increase of gravitational acceleration, especially small gravitational acceleration. By careful observation, it can be concluded that the relationship between bubble departure volume, liquid density and gravitational acceleration is $V_{det} \propto 1/(g\rho_l)$.

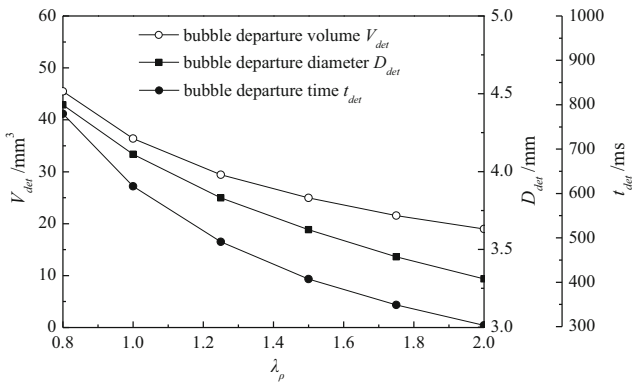


**Fig. 18** Effect of liquid density on bubble departure parameters

## Conclusions

This paper presents an axisymmetric VOSET method for the numerical simulation of quasi-static bubble formation from a submerged orifice in a quiescent viscosity liquid, in combination with the continuum surface force (CSF) model and static contact angle model. The influence of various operating conditions on bubble shape, departure time and departure volume are investigated and analyzed. Based on the detailed analysis and discussion of the numerical results the following conclusions are presented.

1. For quasi-static bubble formation, substantial increase in gas flow rate leads to little increase in bubble departure volume, but results in a large decrease in departure time.
2. Orifice size and surface tension have a positive liner relationship with the capillary force resisting bubble detachment. Thus, the increase of orifice size and surface tension results in the linear increase of bubble departure volume which produces large buoyancy force to overcome the capillary force.
3. There is a critical value of contact angle. When contact angle is smaller than the critical value, contact

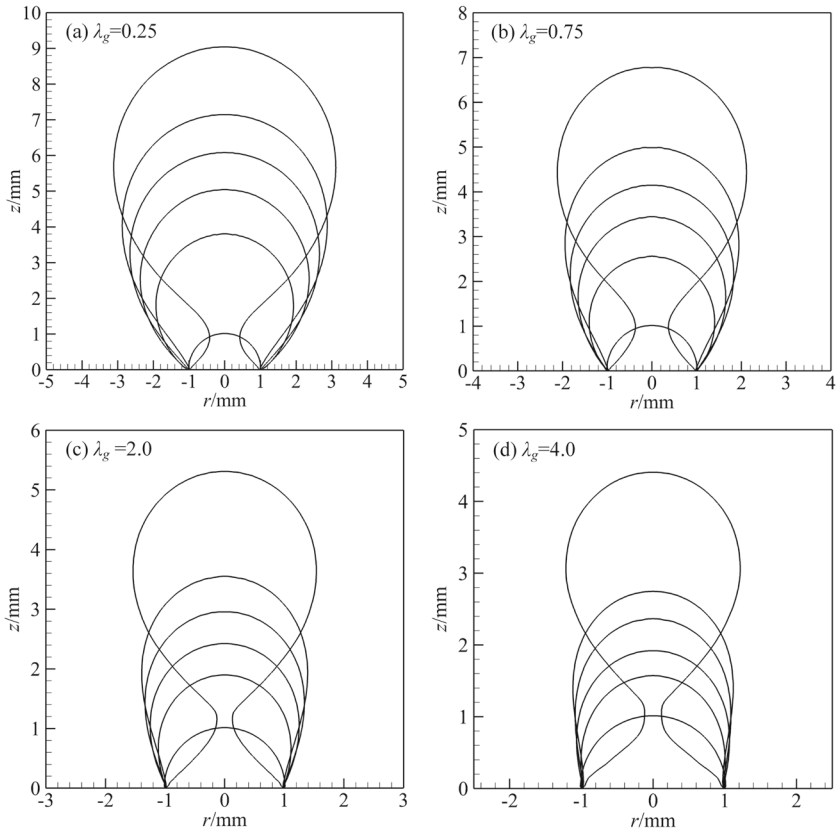


**Fig. 19** Bubble shapes at different time $t/t_{det}$ = 0, 0.2, 0.4, 0.6, 0.8, 1.0 for different gravitational acceleration

angle has no significance effect on the capillary force, thus bubble departure volume nearly keeps unchanged with the increase of contact angle. And, the contact line is nearly fixed on the orifice edge. But, when contact angle is larger than the critical value, increase in contact angle leads to quickly increase in bubble departure volume, and the contact line quickly moves away from the orifice edge.

4. With the increase of liquid density and gravitational acceleration, achieving the same buoyancy force need a smaller bubble volume. Thus, it leads to a smaller bubble departure volume, but the decrease amplitude gradually decreases.
5. At the stage of bubble detachment, bubble bottom gradually becomes a neck shape, and the position of the smallest part of the neck approximately equals to the orifice radius $R_c$.

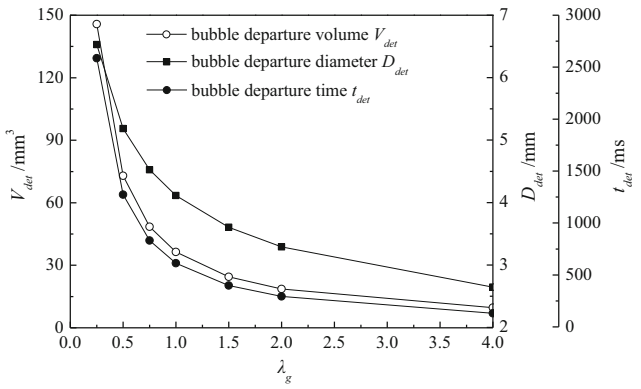


**Fig. 20** Effect of gravitational acceleration on bubble departure parameters

**Acknowledgments** The present study is supported financially by the Fundamental Research Funds for the Central Universities (2018MS105) and the joint fund between the Chinese Academy of Sciences (CAS) and National Natural Science Foundation of China (NSFC) under the grant of U1738105.



## References

Albadawi, A., Donoghue, D.B., Robinson, A.J., Murray, D.B., Delauré, Y.M.C.: Influence of surface tension implementation in volume of fluid and coupled volume of fluid with level set methods for bubble growth and detachment. Int. J. Multiphase Flow. **53**, 11–28 (2013)

Arias, S., Montlaur, A.: Influence of contact angle boundary condition on CFD simulation of T-junction. Microgravity Sci. Technol. **30**, 435–443 (2018)

Badam, V.K., Buwa, V., Durst, F.: Experimental investigations of regimes of bubble formation on submerged orifices under constant flow condition. Can. J. Chem. Eng. **85**, 257–267 (2007)

Bitlloch, P., Ruiz, X., Ramírez-Piscina, L., Casademunt, J.: Bubble dynamics in turbulent duct flows: lattice-boltzmann simulations and drop tower experiments. Microgravity Sci. Technol. **30**, 525–534 (2018)

Brackbill, J.U., Kothe, D.B., Zemach, C.: A continuum method for modeling surface tension. J. Comput. Phys. **100**, 335–354 (1992)

Buwa, V.V., Gerlach, D., Durst, F., Schlücker, E.: Numerical simulations of bubble formation on submerged orifices: Period-1 and period-2 bubbling regimes. Chem. Eng. Sci. **62**, 7119–7132 (2007)

Chakraborty, I., Biswas, G., Polepalle, S., Ghoshdastidar, P.S.: Bubble formation and dynamics in a quiescent high-density liquid. AICHE J. **61**, 3996–4012 (2015)

Chakraborty, I., Ray, B., Biswas, G., Durst, F., Sharma, A., Ghoshdastidar, P.S.: Computational investigation on bubble detachment from submerged orifice in quiescent liquid under normal and reduced gravity. Phys. Fluids. **21**, 062103 (2009)

Chen, Y., Mertz, R., Kulenovic, R.: Numerical simulation of bubble formation on orifice plates with a moving contact line. Int. J. Multiphase Flow. **35**, 66–77 (2009)

Das, A.K., Das, P.K., Saha, P.: Formation of bubbles at submerged orifices - experimental investigation and theoretical prediction. Exp. Thermal Fluid Sci. **35**, 618–627 (2011)

Di Bari, S., Robinson, A.J.: Experimental study of gas injected bubble growth from submerged orifices. Exp. Thermal Fluid Sci. **44**, 124–137 (2013)

Georgoulas, A., Koukouvinis, P., Gavaises, M., Marengo, M.: Numerical investigation of quasi-static bubble growth and detachment from submerged orifices in isothermal liquid pools: the effect of varying fluid properties and gravity levels. Int. J. Multiphase Flow. **74**, 59–78 (2015)

Gerlach, D., Alleborn, N., Buwa, V., Durst, F.: Numerical simulation of periodic bubble formation at a submerged orifice with constant gas flow rate. Chem. Eng. Sci. **62**, 2109–2125 (2007)

Gerlach, D., Biswas, G., Durst, F., Kolobaric, V.: Quasi-static bubble formation on submerged orifices. Int. J. Heat Mass Transf. **48**, 425–438 (2005)

Guo, D.Z., Sun, D.L., Li, Z.Y., Tao, W.Q.: Phase change heat transfer simulation for boiling bubbles arising from a vapor film by the VOSET method. Numer. Heat. Transfer A-Appl. **59**, 857–881 (2011)

Hanafizadeh, P., Eshraghi, J., Kosari, E., Ahmed, W.H.: The effect of gas properties on bubble formation, growth, and detachment. Part. Sci. Technol. **33**, 645–651 (2015)

Hirt, C.W., Nichols, B.D.: Volume of fluid (VOF) method for the dynamics of free boundaries. J. Comput. Phys. **39**, 201–225 (1981)

Kim, D.E., Yu, D.I., Jerng, D.W., Kim, M.H., Ahn, H.S.: Review of boiling heat transfer enhancement on micro/nanostructured surfaces. Exp. Thermal Fluid Sci. **66**, 173–196 (2015)

Lesage, F.J., Cotton, J.S., Robinson, A.J.: Modelling of quasi-static adiabatic bubble formation, growth and detachment for low bond numbers. Chem. Eng. Sci. **104**, 742–754 (2013)

Lesage, F.J., Marois, F.: Experimental and numerical analysis of quasi-static bubble size and shape characteristics at detachment. Int. J. Heat Mass Transf. **64**, 53–69 (2013)

Ma, D., Liu, M., Zu, Y., Tang, C.: Two-dimensional volume of fluid simulation studies on single bubble formation and dynamics in bubble columns. Chem. Eng. Sci. **72**, 61–77 (2012)

Mirsandi, H., Rajkotwala, A.H., Baltussen, M.W., Peters, E.A.J.F., Kuipers, J.A.M.: Numerical simulation of bubble formation with a moving contact line using local front reconstruction method. Chem. Eng. Sci. **187**, 415–431 (2018)

Movafaghian, S., Jaua-Marturet, J.A., Mohan, R.S., Shoham, O., Kouba, G.E.: The effects of geometry, fluid properties and pressure on the hydrodynamics of gas-liquid cylindrical cyclone separators. Int. J. Multiphase Flow. **26**, 999–1018 (2000)

Munro, T.R., Ban, H.: Flow and heat flux behavior of micro-bubble jet flows observed in thin, twisted-wire, subcooled boiling in microgravity. Microgravity Sci. Technol. **27**, 49–60 (2015)

Oguz, H.N., Prosperetti, A.: Dynamics of bubble growth and detachment from a needle. J. Fluid Mech. **257**, 111–145 (1993)

Osher, S., Sethian, J.A.: Fronts propagating with curvature-dependent speed: algorithms based on Hamilton-Jacobi formulations. J. Comput. Phys. **79**, 12–49 (1988)

Pang, M.J., Wei, J.J., Yu, B.: Investigation on effect of gravity level on bubble distribution and liquid turbulence modification for horizontal channel bubbly flow. Microgravity Sci. Technol. **29**, 313–324 (2017)

Shi, D.X., Bi, Q.C., Zhou, R.Q.: Numerical simulation of a falling ferrofluid droplet in a uniform magnetic field by the VOSET method. Numer. Heat. Transfer A-Appl. **66**, 144–164 (2014)

Simmons, J.A., Sprittles, J.E., Shikhmurzaev, Y.D.: The formation of a bubble from a submerged orifice. Eur. J. Mech. B-Fluid. **53**, 24–36 (2015)

Sun, D.L., Tao, W.Q.: A coupled volume-of-fluid and level set (VOSET) method for computing incompressible two-phase flows. Int. J. Heat Mass Transf. **53**, 645–655 (2010)

Sussman, M., Puckett, E.G.: A coupled level set and volume-of-fluid method for computing 3D and axisymmetric incompressible two-phase flows. J. Comput. Phys. **162**, 301–337 (2000)

Vafaei, S., Borca-Tasciuc, T., Wen, D.S.: Theoretical and experimental investigation of quasi-steady-state bubble growth on top of submerged stainless steel nozzles. Colloid Surface A. **369**, 11–19 (2010)

Wang, T., Li, H.X., Li, Y.: Numerical investigation on coaxial coalescence of two gas bubbles. J. Xi'an Jiaotong Univ. **47**, 1–6 (2013)

Wang, T., Li, H.X., Zhao, J.F.: Three-dimensional numerical simulation of bubble dynamics in microgravity under the influence of nonuniform electric fields. Microgravity Sci. Technol. **28**, 133–142 (2016)

Wu, K., Li, Z.D., Zhao, J.F., Li, H.X., Li, K.: Partial nucleate pool boiling at low heat flux: preliminary ground test for SOBER-SJ10. Microgravity Sci. Technol. **28**, 165–178 (2016)

Wu, W.B., Liu, Y.L., Zhang, A.M.: Numerical investigation of 3D bubble growth and detachment. Ocean Eng. **138**, 86–104 (2017)

Youngs, D.L.: Time-dependent multi-material flow with large fluid distorion. In: Morton, K.W., Baines, M.J. (eds.) Numerical Methods for Fluid Dynamics. Acadimic Press, New York (1982)

Zhang, L., Shoji, M.: Aperiodic bubble formation from a submerged orifice. Chem. Eng. Sci. **56**, 5371–5381 (2001)

Zhang, Y.J., Liu, M.Y., Xu, Y.G., Tang, C.: Three-dimensional volume of fluid simulations on bubble formation and dynamics in bubble columns. Chem. Eng. Sci. **73**, 55–78 (2012)

Zhang, Y.H., Liu, B., Zhao, J.F., Deng, Y.P., Wei, J.J.: Experimental study of subcooled flow boiling heat transfer on a smooth surface in short-term microgravity. Microgravity Sci. Technol. **30**, 793–805 (2018)